Joint estimation of activity and attenuation in PET/MR using MR-constrained Gaussian priors

Abolfazl Mehranian, *Student Member, IEEE* and Habib Zaidi†, *Senior Member, IEEE*

***Abstract*– The maximum likelihood estimation of attenuation and activity (MLAA) has been proposed to jointly estimate activity and attenuation from emission data only. In this paper, we proposed an improved MLAA algorithm by imposing MR spatial and CT statistical constraints on the estimation of attenuation using a constrained Gaussian mixture model (GMM) and a Markov random field (MRF) smoothness prior. We compare the proposed MLAA-GMM algorithm with the MLAA algorithms proposed by Rezaei *et al* and Salomon *et al* as well as 4-class MRAC method. Dixon MR images were segmented into outside air, fat and soft tissue classes and an MR low-intensity class corresponding to air cavities, bone and susceptibility artifacts. To eliminate the miss-classification of bones with surrounding tissue, the unknown class was expanded by a co-registered bone probability map. A mixture of 4 Gaussians (air, fat/soft and bone) was used for the unknown class, while unimodal Gaussians were used for others. The algorithms were evaluated using simulation and clinical datasets. The bias in estimated attenuation and activity was evaluated against CT-based attenuation correction. Our results show that MLAA-Rezaei suffers from scale and noise problems. The performance of MLAA-Salomon algorithm is also affected by the scale and depends highly on MR quality and segmentation, especially at air/bone interfaces and vertebra. It was demonstrated the MLAA-GMM effectively exploits MR prior information, thereby results in noise-, crosstalk- and scale-free attenuation maps. The PET bias analyses showed that the MLAA-GMM outperformed the scale corrected MLAA-Rezaei and MLAA-Salomon algorithms as well as the 4-class MRAC method. Therefore, the proposed method can pave the way toward accurate emission-based estimation of attenuation in TOF PET/MR imaging.**

I. Introduction

MR-based attenuation correction (MRAC) in quantitative PET/MR imaging is a challenging task, owing to the lack of bone signal in conventional MR sequences, as well as, a unique global mapping between MR intensities and 511-keV attenuation maps. Recently, it has been shown that attenuation maps can be directly estimated from time-of-flight (TOF) emission data by joint maximum likelihood reconstruction of attenuation and activity (MLAA) [1]. Generally, the performance of the MLAA depends on i) TOF timing resolution in order to suppress cross-talk artifacts between activity and attenuation maps, ii) the count statistics of emission data for suppressing noisy estimations and iii) the spatial distribution of radiotracer over the body to support the estimation of attenuation. In [2], Salomon *et al* proposed a region-wise estimation of attenuation over MR-derived anatomical regions to reduce the number of attenuation's unknowns and crosstalk artifacts. However, in conventional MR sequences, bones cannot be well discriminated from air, and the images are usually suffer from partial volume effect (PVE) leading to the classification of bones in surrounding tissues. Depending on the number of regions, the region-wise estimation also might not allow for attenuation heterogeneity, especially in lungs and vertebra.

In this study, we aimed at improving the performance of MLAA by exploiting segmented Dixon MR images and a co-registered bone probability map (BPM) in order to define spatial and statistical constraints on the estimation of attenuation using a constrained Gaussian mixture model (GMM) and Markov random field (MRF) smoothness prior. The proposed algorithm was compared with MLAA, Salomon's MLAA and the conventional 4-class MRAC method.

II. Material and Methods

A. Objective function

The measured TOF PET data, g_{it}, in LOR i and time bin t are best modeled as Poisson random variables with expected value:

$$\bar{g}_{it} = n_i e^{-\sum_{k=1}^{J} l_{ik}\mu_k} \sum_{j=1}^{J} c_{ijt}\lambda_j + n_i \bar{s}_{it} + \bar{r}_i, \quad (1)$$

where λ_j and μ_k are activity and attenuation values at voxels j and k, c_{ijt} is the geometric probability detection of annihilation events emitted from voxel j along LOR i in TOF bin t, n_i is detector normalization factors, l_{ik} is the intersection length of LOR i with voxel k, and $\bar{s}_{it}$ and $\bar{r}_i$ are the estimates of scatter and random events, estimated by model-based methods and delayed coincidence window measurements, respectively. In maximum a posteriori framework, the unknowns λ and μ are also modeled as random variables with prior densities, by which the solution space can be constrained. We exploited a priori knowledge about attenuation in the following joint estimation:

$$(\hat{\lambda}, \hat{\mu}) = \underset{\lambda\geq 0, \mu\geq 0}{\operatorname{argmax}} \Big\{ \sum_{it} \{ g_{it} \log(\bar{g}_{it}) - \bar{g}_{it} \} + \beta R_{MRF}(\mu) + \gamma R_{GMM}(\mu) \Big\} \quad (2)$$

where R_{MRF} and R_{GMM} are MRF and Gaussian mixture penalties to favor attenuation maps that are smooth and belong to a few distinct tissue classes. β and γ are hyper-parameters. $R_{MRF}(\mu)$ is defined as:

$$R_{MRF}(\mu) = -\sum_{j=1}^{J} \sum_{k\in N_j} \omega_{jk}\, \psi(\mu_k - \mu_j), \psi(t) = \frac{1}{2}t^2, \quad (3)$$

where N_j denotes a neighborhood around jth voxel, ω_{jk} is inversely proportional to the distance between voxel j and k, and $\psi(t)$ is a quadratic potential function penalizing large differences between voxels. In $R_{GMM}(\mu)$, it is assumed that the attenuation values are independent random variables with a density function that is a mixture of H known Gaussian density functions:

$$R_{GMM}(\mu) = \sum_{j=1}^{J} \log\{\sum_{h=1}^{H} \pi_h \mathcal{N}(\mu_j | \bar{\mu}_h, \sigma_h)\},$$
$$\mathcal{N}(\mu_j | \bar{\mu}_h, \sigma_h) = \frac{1}{\sqrt{2\pi}\sigma_h} \exp\left(-\frac{1}{2}\left(\frac{\mu_j - \bar{\mu}_h}{\sigma_h}\right)^2\right). \quad (4)$$

where $\mathcal{N}(\mu_j | \bar{\mu}_h, \sigma_h)$ is the Gaussian density function associated with the hth component with mean $\bar{\mu}_h$ and standard deviation σ_h, $\{\pi_h\}$ are mixture proportions that are assumed to be known and $\sum_h \pi_h = 1$. The mixture of Gaussians is used to reflect the fact that the histogram of attenuation maps is generally consists of a few distinct peaks corresponding to air, lung, fat, soft tissue and bone [3]. In this work, we incorporated spatial information derived from Dixon MR images into the GMM using a tissue prior map.

A. Mehranian is with Division of Nuclear Medicine and Molecular Imaging, Geneva University Hospital, CH-1211 Geneva, Switzerland (e-mail: abolfazl.mehranian@etu.unige.ch).

†H. Zaidi is with the Division of Nuclear Medicine and Molecular Imaging, Geneva University Hospital, CH-1211 Geneva, Switzerland, Geneva, Neuroscience Center, Geneva University, CH-1205 Geneva, Switzerland, and Department of Nuclear Medicine and Molecular Imaging, University of Groningen, University Medical Center Groningen, Groningen, Netherlands (e-mail: habib.zaidi@hcuge.ch).

978-1-4799-6097-2/14/$31.00 ©2014 IEEE

B. Tissue prior map and GMM parameters

As shown in Fig. 1, in contrary to Salomon's work in this study, MR images are segmented into four known classes (outside air, lung, fat, soft) and an unknown class indicating the regions of low MR intensity, corresponding to air gaps, cortical bones and susceptibility artifacts. A co-registered BPM is added to the unknown class to eliminate the misclassification of bones due to PVE. In the proposed MLAA-GMM, a mixture of Gaussians is used for the estimation of attenuation over the unknown class, while uni-modal Gaussians are used for known tissue classes. The whole-body CT images of 10 patients were used to estimate the parameters of uni-modal Gaussians that best fit the histogram of attenuation values in known tissue classes, as well as, those of a mixture of 4 Gaussians for the unknown class, representing inside air, fat/soft mixture and bone. Table I summarizes the estimated parameters of the Gaussian models.

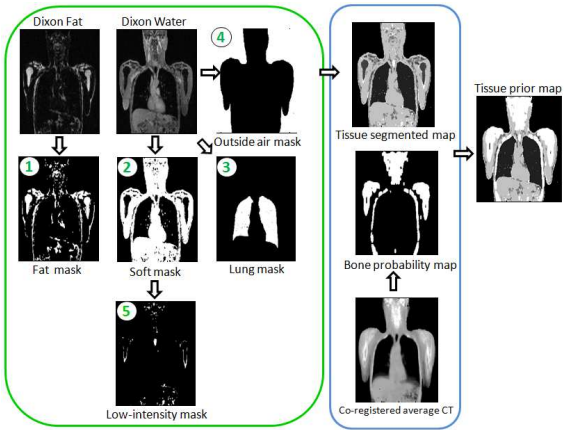

Fig 1. Derivation of tissue prior map from Dixon MR and co-registered CT images.

TABLE I. Estimated parameters of the constrained GMM over 10 whole-body CT images.

MIXTURE OF GAUSSIANS			UNI-MODAL GAUSSIANS		
$\bar{\mu}$	σ	π		$\bar{\mu}$	σ
0.1205	0.0242	0.5661	LUNG	0.0261	0.0107
0.0980	0.0051	0.2597	FAT	0.0834	0.0013
0.0278	0.0330	0.1150	SOFT	0.0954	0.0012
0.0023	0.0019	0.0592			

C. Optimization

The problem in (2) was optimized using optimization transfer and alternating maximization as follows [4]:

$$a_i^n = e^{-\sum_j l_{ij}\mu_j^n} \tag{5}$$

$$\lambda_j^{n+1} = \frac{\lambda_j^n}{\sum_i c_{ij} n_i a_i^n} \sum_{it} c_{ijt} n_i a_i^n \frac{g_{it}}{n_i a_i^n \sum_k c_{ikt}\lambda_k^n + n_i \bar{s}_{it} + \bar{r}_i} \tag{6}$$

$$\psi_i^n = n_i a_i^n \sum_{jt} c_{ijt} \lambda_j^{n+1} \tag{7}$$

$$z_{jh}^n = \frac{\pi_h \mathcal{N}\left(\mu_j^n \middle| \bar{\mu}_h, \sigma_h\right)}{\sum_q \pi_q \mathcal{N}\left(\mu_j^n \middle| \bar{\mu}_q, \sigma_q\right)} \tag{8}$$

$$\mu_j^{n+1} = \mu_j^n + \alpha \left(\frac{\sum_i l_{ij} \frac{\psi_i^n}{\psi_i^n + b_i} (\psi_i^n + b_i - g_i) - \gamma \sum_h z_{jh}^n \frac{\mu_j^n - \bar{\mu}_h}{(\sigma_h)^2} - \beta \frac{\partial R_{MRF}(\mu^n)}{\partial \mu_j}}{\sum_j l_{ij} \frac{(\psi_i^n)^2}{\psi_i^n + b_i} \sum_k l_{ik} - \gamma \sum_h \frac{z_{jh}^n}{(\sigma_h)^2} + \beta \frac{\partial^2 R_{MRF}(\mu^n)}{\partial^2 \mu_j}} \right), \tag{9}$$

where $b_i = n_i \bar{s}_i + \bar{r}_i$, $c_{ij} = \sum_t c_{ijt}$, $g_i = \sum_t g_{it}$ and $\bar{s}_i = \sum_t \bar{s}_{it}$ are time-integrated quantities and $\alpha > 0$ is a step size parameter. z_{jh}^n is obtained from the expectation maximization of GMM and defines the membership probability of μ_j^n to class h. In a known class, $z_{jh}^n = 1$ and 0 elsewhere, thus GMM is constrained to a uni-modal Gaussian in that class. For both simulation and clinical studies reported in this work, we set $\alpha = 1.5, \beta = 50, \gamma = 0.015$.

D. Evaluation using simulated and clinical studies

A clinical FDG thorax PET/CT/MR dataset was used to simulate a 80 and 20 M-count data acquisitions on the Philips ingenuity PET/MR scanner with TOF time resolution of 580 ps and perfect correction for random and scatter coincidences. The 4D sinograms had 291 radial bins, 168 angles, 241 planes and 19 time bins of 210.5 ps width. Activity and attenuation maps were simultaneously reconstructed with matrix size of 288×288×87. For the clinical evaluation of the algorithms, a patient with head and neck carcinoma was injected with 280 MBq of ^{18}F-FDG and scanner on the Biograph mCT flow scanner (Siemens Healthcare) and Ingenuity TF PET/MRI scanner (Philips Healthcare). TOF-PET data of the mCT scanner were used for reconstruction of activity and attenuation maps and the co-registered MR images of the PET/MR scanner were used for MRI-guided 4-class based attenuation correction and the MLAA algorithm. The 4D TOF sinograms of mCT had 400 radial bins, 168 azimuthal angles, 621 planes (in 9 segments with span 11) and 13 time bins of 312 ps width. The attenuation and activity were reconstructed for a single bed with matrix size of 400×400×109. For MLAA-Salomon, the in-phase MR image was segmented into many regions using a hybrid *k*-means and Markov random field clustering algorithm by means of the VolView software (Kitware, Inc., Clifton Park, NY), followed by connected component labeling. Regions with less than 10 voxels were assigned to their nearest populated regions. An initial attenuation map was derived by filling the body contour with water attenuation value (0.0957 cm^{-1}). Fig 2 shows the simulation PET/CT/MRI dataset, plus 4-class attenuation map, MR regions used in Salomon's method and tissue prior map used in our method.

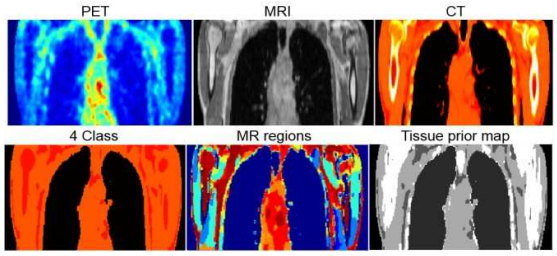

Fig. 2 The FDG PET/CT/MR dataset and the MR-derived attenuation and prior maps.

III. RESULTS

A. Simulation studies

The attenuation map of the simulation dataset was estimated by the MLAA algorithms using 50 global iterations, 1 iteration, 4 subsets for activity and 1 iteration, 7 subsets for attenuation. It was found that as the number of global iterations increases, the bias in attenuation maps decreases, however, activity maps become noisy. Hence, final activity maps were post-reconstructed by an OSEM algorithm with 15 iteration, 4 subsets. The attenuation maps of MLAA algorithm were smoothed by a 3D Gaussian filter, 3 mm in FWHM, before the final activity reconstruction. Fig. 3 compares the estimated attenuation maps with the true CT map. As seen, the proposed algorithm has substantially suppressed noise compared to MLAA and well differentiated bones compared to MLAA-Salomon.

Fig. 4 shows the mean ± standard deviation of estimated LACs from CTAC with global iteration number in soft tissue, lung and bone classes. The results show that as iteration increases the estimated LACs get closer to true values, especially in the lung. However, for the MLAA, noise extensively increases. In general, the proposed algorithm can outperform the algorithms by achieving the lowest absolute bias-variance. Table II summarizes the PET quantification errors (%Bias) of the algorithms in soft/fat, lung and bone classes for both high and low count simulations with respect to the reference PET-CTAC images. The results shows that the proposed MLAA-GMM achieves a better absolute bias, especially in soft tissue and

lungs. The results also show that in the lower counts the algorithms induced more bias; however, the bias performance of the MLAA and MLAA-Salomon algorithms depends on count level more than the proposed MLAA algorithm.

TABLE II. % Bias in reconstructed activity maps of the simulated thorax dataset.

Counts	Region	4 Class	MLAA	MLAA-Salomon	MLAA-GMM
	Fat+Soft	–5.2 ± 15.8	12.1 ±19.5	7.8 ± 17.6	3.6 ±13.3
	Lung	–23.1 ±13.7	23.2 ±19.8	14.5 ± 26.9	6.8 ±13.9
8×10^7	Bone	–24.5 ±14.1	6.5 ±18.3	–6.3 ± 16.1	–4.6 ±12.6
	Fat+Soft	–3.6 ± 21.9	21.3 ± 39.5	15.4 ± 23.2	4.4 ± 19.9
	Lung	–17.1 ± 21.9	45.6 ± 53.2	25.4 ± 27.1	14.1 ± 23.1
2×10^7	Bone	–25.6 ± 21.9	12.9 ± 37.5	5.2 ± 21.2	–9.3 ± 15.1

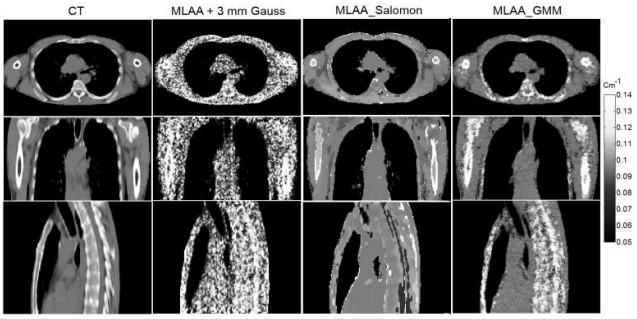

Fig. 3 The comparison of the estimated attenuation maps with the true CT-based map.

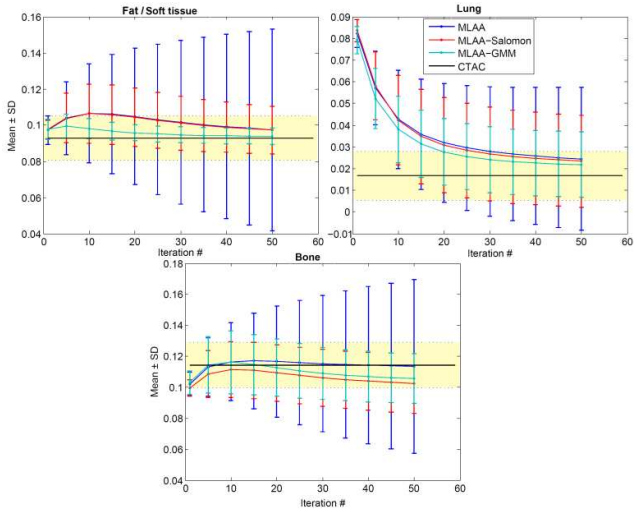

Fig. 4 The mean ± standard deviation of estimated LACs from CTAC with iteration number in fat/soft tissue, lung and bone classes. The yellow bars show the two-sigma variation of LACs in CTAC.

B. Clinical studies

For the clinical dataset, the activity and attenuation pair were reconstructed using 40 global iterations, 1 iteration and 2 subsets for activity updates followed by 1 iteration and 3 subsets for attenuation updates. In this dataset, the CT-based scatter component was employed in the MLAA algorithms. The reference CTAC-PET image was reconstructed using TOF-OSEM algorithm for 35 iterations and 2 subsets. It has been theoretically and experimentally shown that attenuation maps or attenuation correction factors can be estimated from TOF emission data up to a constant factor. To solve the scaling problem, Rezaei *et al* [1] iteratively imposed the known value of tissue attenuation to the 75th percentile of the LACs within the body contour. In this clinical dataset, we evaluated the MLAA and MLAA-Salomon algorithms both with and without scale correction (SC) using the method proposed in [1].

Fig. 5 compares the reconstructed attenuation maps with the reference CTAC attenuation map as well as the corresponding in-phase MR image used in MLAA-Salomon-SC and MLAA-GMM algorithms. In this comparison, the attenuation maps were smoothed using a 5 mm FWHM 3D Gaussian filter. The results show that the MLAA-SC attenuation map suffers from noise as well as normalization correction artifacts due to incorrect expansion of normalization components in this patient dataset. Salomon's algorithm effectively reduces the noise and artifacts; however, it suffers from MR segmentation errors, especially in the backbone area due to MR field inhomogeneities. In contrast, the proposed algorithm estimates more accurately the attenuation map through effective suppression of noise, artifacts and the scaling of attenuation.

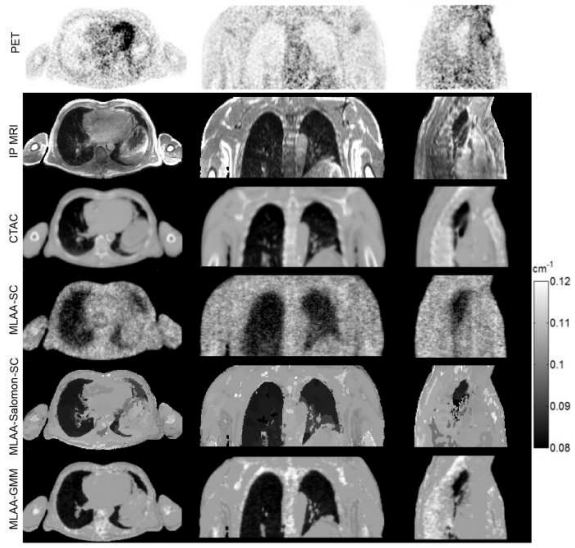

Fig 5. Comparison of the estimated attenuation maps for the ^{18}F-FDG clinical study with the reference CT-based attenuation map and the corresponding PET and MR images.

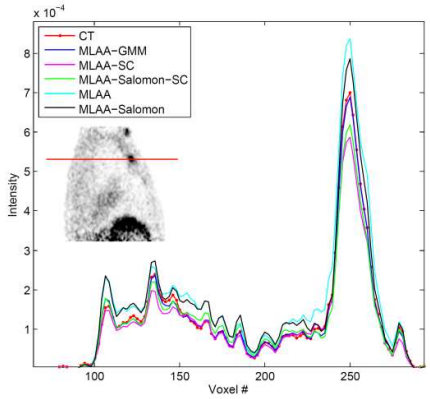

Fig 6. The activity profiles of the MLAA activity maps for the 18F-FDG clinical study compared to their reference CTAC-OSEM profiles

Fig. 6 compares the profiles of the estimated activity maps in this patient with respect to reference CTAC activity map along the depicted lines. As can be seen, the activity profiles of the MLAA and MLAA-Salomon algorithms are scaled and overestimate the hot and background regions. The scale correction of these algorithms using Rezaei's method tends to suppress the overestimation and improves the performance of the algorithms, especially Salomon's method However, since this correction technique is not robust; it underestimates the activity in regions with high uptake. The results show that the proposed method can reliably solve the scaling problem of the joint activity/attenuation estimation.

The bias performance of the algorithms over soft-tissue, lung and bone classes was also evaluated for the MLAA algorithms and 4-class MRAC method. Table III summarizes the results of the bias in

different tissue classes. The results demonstrate that MLAA and MLAA-Salomon suffer from the scaling problem. The scale correction improves the results, but the bias is still high. In comparison, the results of MLAA-GMM are quite satisfactory and demonstrate the potential outperformance of the proposed emission-based method over standard segmentation-based MRAC methods. However, any further conclusion necessitates a comparative study over a larger clinical database.

TABLE III. % Bias in reconstructed activity maps of the clinical thorax dataset.

ALGORITHM	FAT + SOFT	LUNGS	BONES
MLAA	51.8 ± 104.1	98.4 ± 148.2	38.4 ± 75.5
MLAA-SC	–10.4 ± 19.0	19.9 ± 38.9	–17.8 ± 15.5
MLAA-SALOMON	24.9 ± 32.3	47.3 ± 40.6	8.6 ± 22.7
MLAA-SALOMON-SC	–2.1 ± 21.6	18.2 ± 32.2	–17.4 ± 14.9
MLAA-GMM	–0.8 ± 20.2	1.97 ± 22.9	–5.5 ± 19.2
4-CLASS MRAC	–5.1 ± 19.8	–13.4 ± 21.0	–24.3 ± 12.9

IV. CONCLUSION

In this work, an emission-based MRAC algorithm was proposed based on the maximum likelihood reconstruction of activity and attenuation with incorporation of prior MR information using a constrained Gaussian mixture model. The performance of the proposed MLAA-GMM algorithm was evaluated against current state-of-the-art MLAA algorithms using simulation and clinical studies. The results demonstrate that our algorithm is not susceptible to MR segmentation errors and provides a practical solution to the cross-talk and scaling problems of activity and attenuation estimates, through panelizing large deviations of attenuation coefficients from their expected values in each MR tissue class and overall attenuation distribution from its expected histogram.

V. ACKNOWLEDGMENTS

This work was supported by the Swiss National Science Foundation under Grant SNSF 31003A-149957 and the Indo-Swiss Joint Research Programme ISJRP 138866. The authors would like to thank Mike Casey and Judson P. Jones (Siemens Healthcare) for providing and supporting VG50 e7 tools for the CBM mode reconstruction of the mCT Flow scanner.

REFERENCES

[1] A. Rezaei, J. Nuyts, M. Defrise, G. Bal, C. Michel, M. Conti, *et al.*, "Simultaneous reconstruction of activity and attenuation in Time-of-Flight PET," *IEEE Nuclear Science Symposium and Medical Imaging Conference (NSS/MIC),* 2011, pp. 2375-2382.

[2] A. Salomon, A. Goedicke, B. Schweizer, T. Aach, and V. Schulz, "Simultaneous Reconstruction of Activity and Attenuation for PET/MR," *IEEE Trans Med Imaging,* vol. 30, pp. 804-813, 2011.

[3] J. M. M. Anderson, K. Yoon-Chul, and J. T. Votaw, "Concurrent Segmentation and Estimation of Transmission Images for Attenuation Correction in Positron Emission Tomography," *IEEE Trans Nucl Sci,* vol. 56, pp. 136-146, 2009.

[4] J. Nuyts, P. Dupont, S. Stroobants, R. Benninck, L. Mortelmans, and P. Suetens, "Simultaneous maximum a posteriori reconstruction of attenuation and activity distributions from emission sinograms," *IEEE Trans Med Imaging,* vol. 18, pp. 393-403, 1999.